SENSITIVITY ANALYSIS OF IRRADIANCE IN AGRIVOLTAIC SYSTEMS FOR DIFFERENT CONFIGURATIONS OF THE PHOTOVOLTAIC GENERATOR

Ronald Barrientos Campos[1,2], Mónica Gómez León[1] and Marcelo Pinho Almeida[2]

[1] Facultad de Ciencias, Universidad Nacional de Ingenieria, Lima (Perú)

[2] Instituto de Energia e Ambiente, Universidade de São Paulo, São Paulo (Brasil)

Abstract

This study presents a sensitivity analysis to explore the possibilities offered by different geometric variables of an agrivoltaic system regarding electricity production and irradiance distribution on the ground between module rows. The analysis allows for a qualitative identification of which of these variables tend to exert greater influence on the observed results.

Keywords: agrivoltaics, sensitivity analysis, ground coverage ratio (GCR), energy yield, shading effects

1. Introduction

Agrivoltaics is proposed as a viable alternative to simultaneously produce energy and food, optimizing land use. This technology integrates crop cultivation with photovoltaic generation, addressing the growing demand for food (Russo et al., 2025) and energy (REN21 Secretariat, 2024) driven by population growth (Asa'a et al., 2024), the need for rural electrification (Alegre-Bravo, Stedman, and Anderson, 2025), and the reduction of the carbon footprint (Walston et al., 2022).

Installing photovoltaic modules over crops can provide benefits, such as protection from excessive solar radiation, hail, and evapotranspiration (Semeraro et al., 2024). However, the shadows cast on the ground-level reduces irradiation availability, which can affect crop development (Yavari et al., 2021).

If electric energy production is prioritized, more modules would be installed, reducing the area available for cultivation. In contrast, if agriculture is prioritized, shading would be minimized (Ko et al., 2023) through increased spacing, tilt, or alternative geometries, which would reduce energy production per unit area.

In this context, it is essential to design an agrivoltaic configuration that considers structural variables, such as height, azimuth, tilt, and the ground coverage ratio (GCR) that optimizes electricity generation and minimizes negative effects on crops.

2. Methodology

This study presents a sensitivity analysis of fixed photovoltaic systems for agrivoltaics applications. It evaluates how different configurations of the photovoltaic generator influence electricity production, ground-level irradiance, and the distribution of shadows between rows.

The variables that were analyzed are azimuth (γ), tilt angle (β), ground clearance height (h), and GCR. The combination of these variables affects both annual electricity generation and the irradiance levels and shading patterns between rows.

Python, together with the PySAM library from NREL, was employed to perform simulations for the sensitivity analysis. Each variable was analyzed separately to evaluate its effect on ground irradiance distribution and shading. Subsequently, it was extended to iterative cases exploring a wider range of scenarios to provide a more detailed analysis of electrical production and total irradiation, which is directly related to the reduction of irradiance beneath the modules. A 1 MW bifacial photovoltaic system with a bifaciality factor (bif) of 0.75, installed at latitudes (Φ) 6.07°, 23.5°, and 51.78° South, was used as reference for evaluating electricity production.

Examples of results are presented in Figure 1, which shows the distribution of irradiance on ground level σ_{xt} (W/m²) between two adjacent rows at different heights (h) of modules over the course of a year. In this figure, the X-axis

10.18086/swc.2025.06.29 Available at http://proceedings.ises.org

represents the horizontal distance between the module rows considering their lowest edges, while the Y-axis indicates the annual hours. In addition, l' represents the projection of the module length (l) on the ground, and ΔX denotes the distance from the farthest tip of the shadow (blue area) to the opposite edge. From these data, the *average irradiation on ground level* H_g (kWh/m²·year) is calculated using (eq. 1).

$$H_g = \frac{1}{10}\sum_{x=1}^{10}\sum_{t=1}^{8760}(\sigma_{xt} \times 1\,\text{hour}) \qquad \text{(eq.1)}$$

The electricity production per unit area E_A (kWh/m²·year) is also calculated, where E represents the annual energy output. To this end, the area A of the photovoltaic generator was first determined using (eq. 2), considering the total number of modules N, the ground coverage ratio (GCR), and the area of a single module A_m. Then, using these values, (eq. 3) was applied to obtain E_A.

$$A = \frac{N\,A_m}{GCR} \qquad \text{(eq. 2)}$$

$$E_A = \frac{E}{A} \qquad \text{(eq. 3)}$$

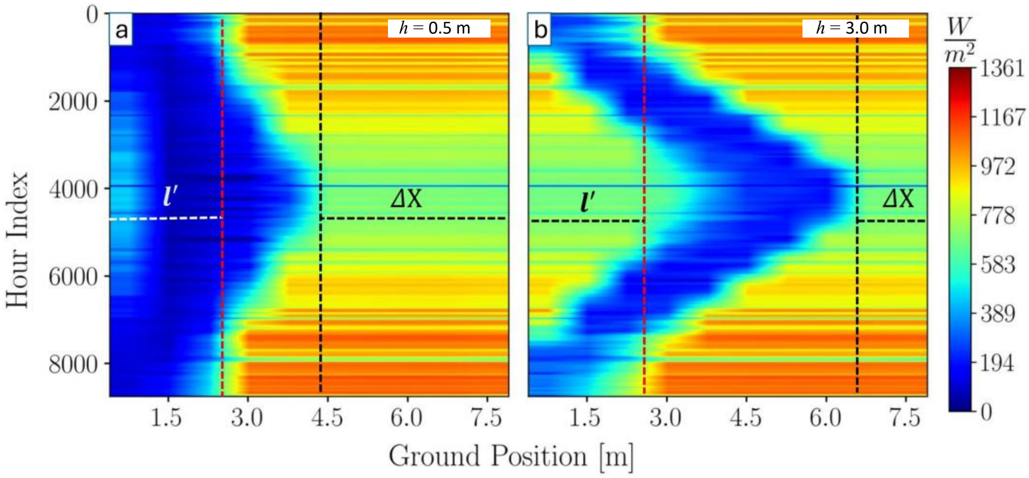

Figure 1: Simulation of irradiance on ground level for Φ = -23.56°, β= 20°, GCR = 0.3, and γ = 0°. The region delimited by the length l' is the area immediately under the modules and the region delimited by the length ΔX is the area with little or no influence of the shadows projected by the modules on the ground level.

It must be considered that configurations generating shading between rows of modules cannot be proposed. For this reason, it is important to consider the row spacing d, which together with the length of modules l defines the GCR (eq. 4). When projecting shadows, the minimum distance d_{min} is commonly used to determine the maximum shadow cast on the ground when the sun is at its lowest position (eq. 5).

$$GCR = \frac{l}{d} \qquad \text{(eq. 4)}$$

$$d_{min} = \frac{h'}{tan(\alpha_c)} + l' = \frac{l.sin(B)}{tan(\alpha_c)} + lcos(\beta) \qquad \text{(eq. 5)}$$

$$\alpha_c = 90° - |\Phi| - 23.5° \qquad \text{(eq. 6)}$$

Where h' is the relative height between the upper and lower edges of the module, α_c is the minimum solar altitude at solar noon. The first term of d_{min} corresponds to the horizontal spacing between the lowest edge of one row and the highest edge of the next row. By relating d_{min} with the GCR, we have that $GCR_{max} = \frac{l}{d_{min}}$, thus obtaining (eq. 7).

$$GCR_{max}(\beta, \Phi) = \frac{sin(\alpha_c)}{sin(\beta+\alpha_c)} \qquad \text{(eq. 7)}$$

Figure 2 shows the curves of GCR_{max} obtained for different latitudes and different tilts. At higher latitudes the GCR_{max} becomes increasingly restricted.

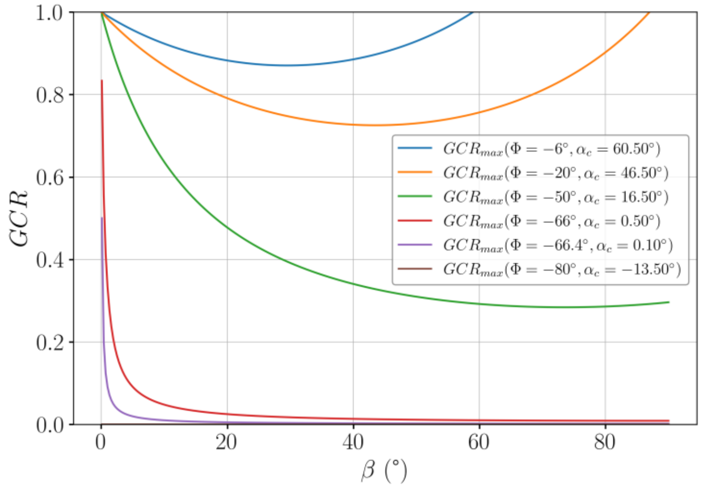

Figure 2: Simulated maximum ground coverage ratio (GCR_{max}) for different latitudes (Φ) and tilts (β).

3. Results

In Sections 3.1, 3.2, 3.3, and 3.4, the results of evaluating ground-level irradiance (σ_{xt}) through single-variable simulations at three different latitudes (−6.07°, −23.56°, and −51.78°) are presented. For clarity and space considerations, only two representative latitudes (−6.07° and −51.78°) are shown in detail. The simulations were performed using the PySAM library of SAM for Python, where σ_{xt} is plotted, and both H_g and E_A are calculated for each case. The parameter configurations for each case (height, azimuth, tilt, and GCR) are summarized in Table 1. In each row only the indicated variable was modified, while the others remained constant. It should be noted that when Φ = 6.07° S, if the resulting tilt β was smaller than 10°, its value was set to 10°. In addition, for the case Φ = 51.78° S, according to Equation (6), the maximum ground coverage ratio is GCR_{max} = 0.28; therefore, GCR = 0.2 was adopted for scenarios where this variable remained constant. Moreover, GCR_2 and GCR_3 represent intermediate values between 0.01 and GCR_{max} for the scenarios where the GCR was analyzed.

Table 1: Parameter configuration for height (h), azimuth (γ), tilt (β), and ground coverage ratio (GCR) used in the simulations. Each row represents a set of simulations in which only the variable indicated in the first column was modified, while the others remained constant.

	$h(m)$	$\gamma(°)$	$\beta(°)$	GCR
Height	1;2;3;10	0	$\|\Phi\|$	0.2 or 0.3
Azimut	2	0;90;180;270	$\|\Phi\|$	0.2 or 0.3
Tilt	2	0	0;30;60;90	0.2 or 0.3
GCR	2	0	$\|\Phi\|$	0.01;GCR_2;GCR_3;GCR_{max}

In addition, for each variable, the graphs of H_g and E_A include a larger number of data points along the X-axis: β = 0°, 10°, 20°, …, 90°; h = 1, 2, 3, …10 m; γ = 0°, 10°, 20°, …, 90°; and GCR = 0.01, $GCR_2, GCR_3, \ldots, GCR_7$, 0.99**.**

3.1 Height

Figures 3 and 5 show the distribution of irradiance on ground level for Φ = 6.07° S and Φ = 51.78° S, respectively. For latitude 6.07° S, it is observed that as h increases, the shadow also extends beyond the module projection l'. This shadow, which appears bluish in color, becomes more diffuse, causing ΔX to decrease until it practically reaches zero.

When analyzing H_g (Figures 4a and 6a), it is observed that H_g does not depend on bif. This occurs because the reflectance of the module's rear surface remains constant. Additionally, H_g decreases as height increases, suggesting that, although the shadows become larger and more diffuse, they reduce ΔX.

For 6.07° S (Figure 4a), H_g follows a bell-shaped curve with a maximum at h = 0 m. This implies that even though the shadow below the module is stronger, it does not significantly affect other areas of the ground. As h increases, the shadow becomes larger but its overall effect diminishes. Although irradiance is reduced over more ground points, the annual irradiation does not decrease substantially. Moreover, for this same latitude, $\Delta H_{g,bif=0} = \Delta H_{g,bif=0.75}$ = 71.93 kWh/m², representing about 5.3% of the minimum value. Similarly, for 51.78° S (Figure 6a), $\Delta H_{g,bif=0} \approx H_{g,bif=0.75}$ = 29.03 kWh/m², corresponding to approximately 3.5% of the minimum.

Furthermore, the electrical energy production per area E_A does not depend on h when bif = 0. This is expected since increasing height only produces a negligible reduction in the distance between the module's upper surface and the Sun, resulting in no significant change in direct or diffuse solar radiation.

For 6.07° S (Figure 4b), the variation range of E_A for bif = 0 remains constant with h, while for bif = 0.75, $\Delta E_{A,bif=0.75}$ = 8.93 kWh/m² (an 8.6% increase relative to the minimum). The bifacial gain $\Delta_{bif} E_A = E_{A,bif=0.75} - E_{A,bif=0}$ ranges from 1.14 to 10.08 kWh/m², representing increases of approximately 1.1% and 9.8%, respectively, relative to bif = 0.

The only component that might vary slightly is the albedo irradiance, but its effect is minimal. However, when considering bif =0.75, the electrical production increases with height.

At 51.78° S (Figure 6b), $\Delta E_{A,bif=0} = 0$ and $\Delta E_{A,bif=0.75} = 0.24\ kWh/m^2$ (0.5%). In this case, $\Delta_{bif} E_A = E_{A,bif=0.75} - E_{A,bif=0}$ varies between 2.08 and 2.32 kWh/m^2, corresponding to relative gains of about 4.8% to 5.3% compared to bif = 0.

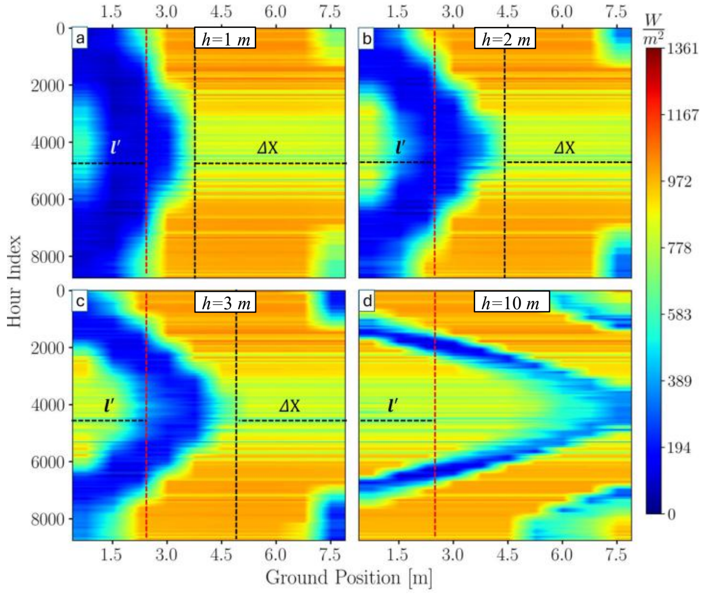

Figure 3: Simulation of irradiance on ground level for a place located at Φ = 6.07° S. The analysis presents the hour index per year for a longitudinal evaluation between two PV rows (β = 10°, GCR = 0.3, γ = 0°, bif = 0.75) with four different heights.

(a) (b)

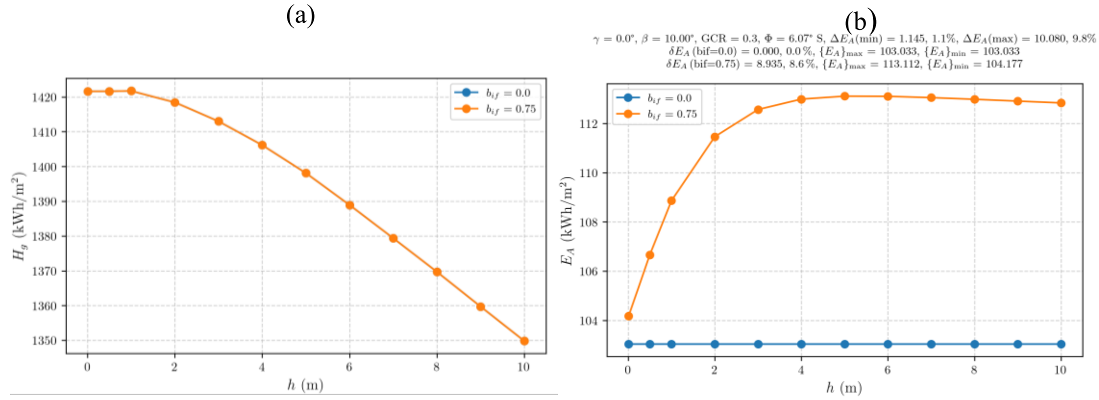

Figure 4: Plot of H_g (a) and E_A(b) vs h for two bifaciality levels, both at Φ = 6.07° S. The analysis shows the annual hour index for a longitudinal evaluation between two PV rows (β = 10°, GCR = 0.3, γ = 0°, bif = 0 (blue line) and 0.75 (orange line), under different heights ranging from 0 m to 10 m.

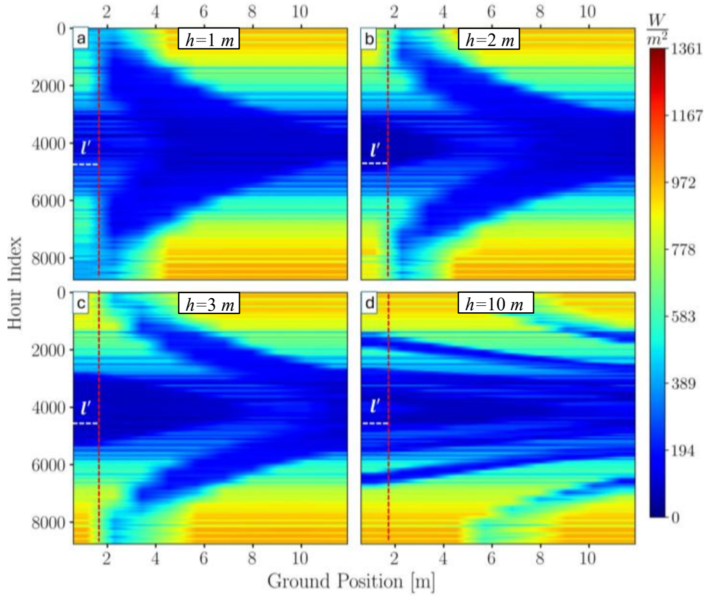

Figure 5: Simulation of irradiance on ground level for a place located at Φ = 51.78° S. The analysis presents the hour index per year for a longitudinal evaluation between two PV rows (*β* = 51.78°, *GCR* = 0.2, γ = 0°, *bif* = 0.75) with four different heights.

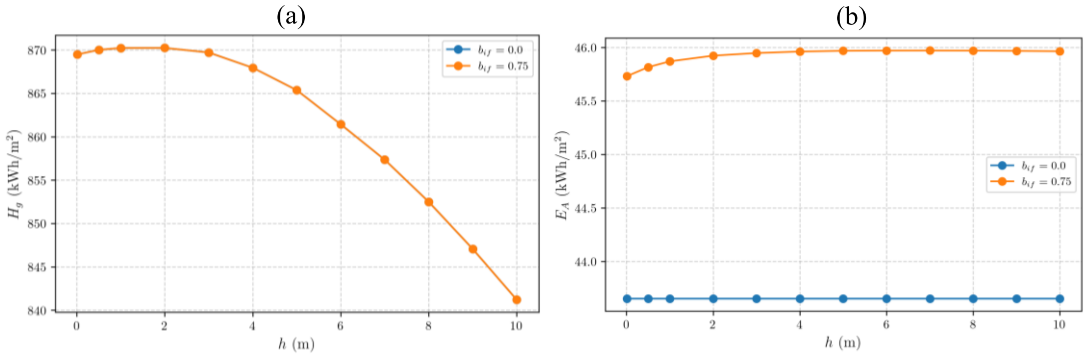

Figure 6: Plot of H_g (a) and E_A (b) vs *h* for two bifaciality levels, both at *Φ* = 51.78° S. The analysis shows the annual hour index for a longitudinal evaluation between two PV rows (*β* = 51.78°, *GCR* = 0.2, γ = 0°, *bif* = 0 (blue line) and 0.75 (orange line), under different heights ranging from 0 m to 10 m.

3.2 Azimuth

At 6.07° S (Figure 7), the shadow gradually changes its orientation as γ varies from 0° (north-facing) to 180° (south-facing), then completing a full 360° rotation. Throughout this range, the shadow length decreases and reaches its minimum near γ = 90° and 270°. A similar trend is observed at higher latitude (51.78° S, Figure 9).

When analyzing H_g in Figures 8 and 10, and considering bif = 0 and 0.75, it is first observed that H_g is again practically unaffected by bifaciality.

For 6.07° S (Figure 8a), H_g follows a bell-shaped curve with a maximum around γ ≈ 200°. Its variation is small, with $\Delta H_{g,bif=0} = \Delta H_{g,bif=0.75} = 14.23\ kWh/m^2$, representing about 1% of the minimum value. Similarly, for 51.78° S (Figure 10a), $\Delta H_{g,bif=0} \approx \Delta H_{g,bif=0.75} = 127.55\ kWh/m^2$, corresponding to approximately 14.7% of the minimum.

Regarding E_A, for 6.07° S (Figure 8b), the variation is $\Delta E_{A,bif=0} = 2.41 kWh/m^2$ (2.4%) and $\Delta E_{A,bif=0.75} = 2.55\ kWh/m^2$ (2.3%). The bifacial gain, defined as $\Delta_{bif} E_A = E_{A,bif=0.75} - E_{A,bif=0}$, ranges from 8.43 to 9.36 kWh/m^2, representing increases of approximately 8.2% and 9.1%, respectively. At 51.78° S (Figure 10b), $\Delta E_{A,bif=0} = 27.70\ kWh/m^2$ (173.8%) and $\Delta E_{A,bif=0.75} = 23.54\ kWh/m^2$ (105.2%). In this case, $\Delta_{bif} E_A$ varies between 2.27 and 6.81 kWh/m^2, corresponding to relative gains of about 5.2% to 31.4%.

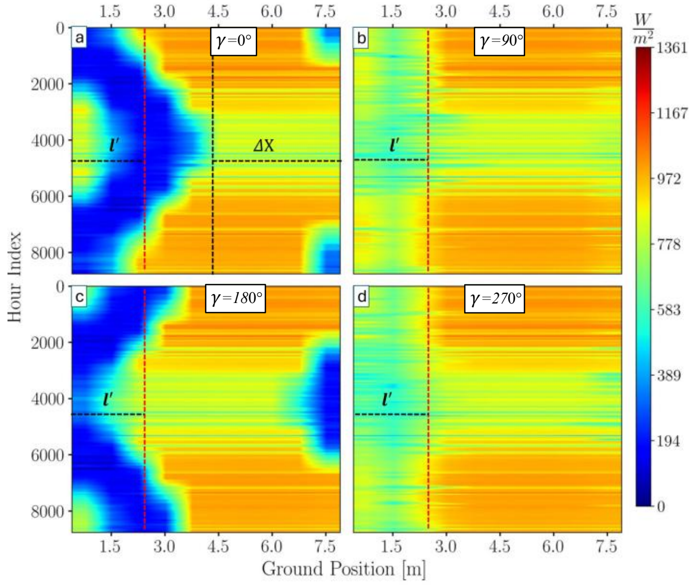

Figure 7: Simulation of irradiance on ground level for a place located at Φ = 6.07° S. The analysis presents the hour index per year for a longitudinal evaluation between two PV rows (β = 10°, GCR = 0.3, h = 2 m, bif = 0.75) with four different azimuths.

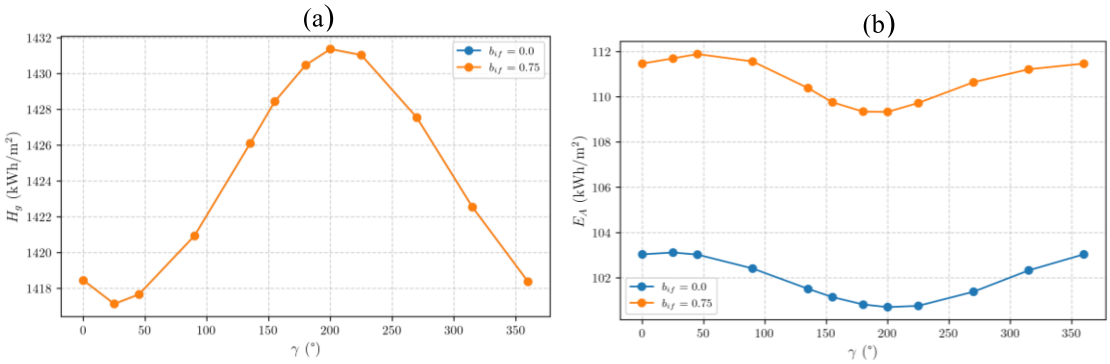

Figure. 8: Plot of H_g (a) and E_A (b) vs γ for two bifaciality levels, both at Φ = 6.07° S. The analysis shows the annual hour index for a longitudinal evaluation between two PV rows (β = 10°, GCR = 0.3, h = 2 m, bif = 0 (blue line) and 0.75 (orange line), under different azimuth angles ranging from 0° to 360°.

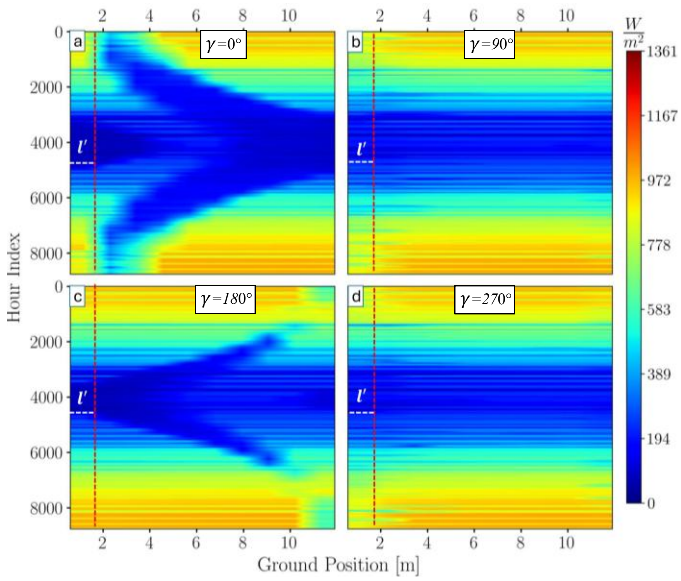

Figure 9: Simulation of irradiance on ground level for a place located at Φ = 51.78° S. The analysis presents the hour index per year for a longitudinal evaluation between two PV rows (β = 51.78°, GCR = 0.3, h = 2 m, *bif* = 0.75) with four different azimuths.

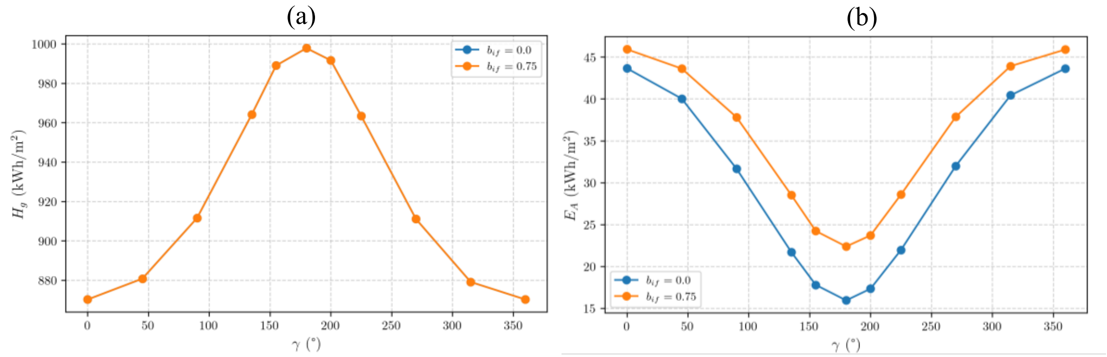

Figure 10: Plot of H_g (a) and E_A (b) vs γ for two bifaciality levels, both at Φ = 51.78° S. The analysis shows the annual hour index for a longitudinal evaluation between two PV rows (β = 51.78°, GCR = 0.3, h = 2 m, bif = 0 (blue line) and 0.75 (orange line), under different azimuth angles ranging from 0° to 360°.

3.3 Tilt

The optimal tilt angle is generally close to the site latitude; however, for locations between 10° S and 10° N, a tilt of around 10° is commonly adopted. At low latitudes (6.07° S), as shown in Figure 11, increasing the tilt progressively reduces shading, with ΔX exhibiting slight fluctuations. This behavior is not observed at higher latitudes, such as 51.78° S (see Figure 13), where only a redistribution of the shadow can be noticed. The shadow pattern becomes elongated during the middle months of the year, indicating periods when the Sun is lower producing longer shadows and others when it is higher resulting in smaller shaded areas. This can be explained by the solar geometry at higher latitudes, where seasonal variations in solar altitude are more pronounced.

For 6.07° S (Figure 12a), H_g follows a bell-shaped curve with a maximum around $\beta \approx 90°$. Its variation is $\Delta H_{g,bif=0} \approx \Delta H_{g,bif=0.75} = 3329.37\ kWh/m^2$, representing about 6.3% of the minimum value. Similarly, for 51.78° S (Figure 14a), $\Delta H_{g,bif=0} \approx \Delta H_{g,bif=0.75} = 65.12\ kWh/m^2$, corresponding to approximately 7.5% of the minimum.

Regarding E_A, for 6.07° S (Figure 12b), the variation is $\Delta E_{A,bif=0} = 64.80\ kWh/m^2$ (169.5% of minimum) and $\Delta E_{A,bif=0.75} = 52.858\ kWh/m^2$ (90.2%). The bifacial gain, defined as $\Delta_{bif}E_A = E_{A,bif=0.75} - E_{A,bif=0}$, ranges from 7.91 to 20.38 kWh/m^2, representing increases of approximately 7.7% and 53.3%, respectively of bif = 0. At 51.78° S (Figure 14b), $\Delta E_{A,bif=0} = 64.80\ kWh/m^2$ (169.5%) and $\Delta E_{A,bif=0.75} = 52.85\ kWh/m^2$ (90.2%). In this case, $\Delta_{bif}E_A$ varies between 7.91 and 20.38 kWh/m^2, corresponding to relative gains of about 1.2% to 19.4% respectively of bif = 0.

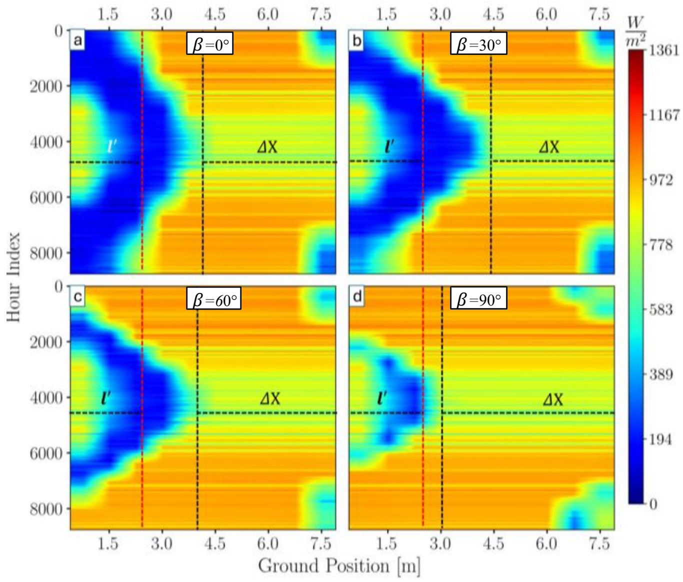

Figure 11: Simulation of irradiance on ground level for a place located at Φ = 6.07° S. The analysis presents the hour index per year for a longitudinal evaluation between two PV rows (h = 2 m, GCR = 0.3, γ = 0°, bif = 0.75) with four different tilts.

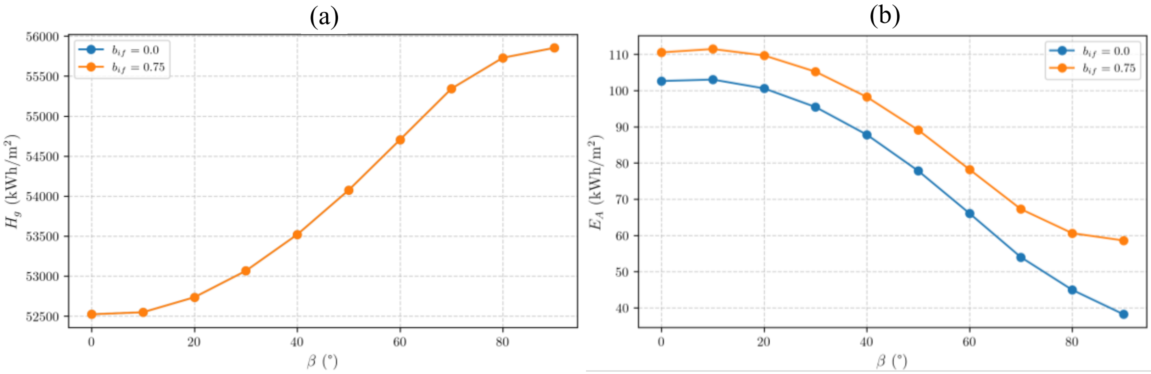

Figure 12: Plot of H_g (a) and E_A (b) vs β for two bifaciality levels, both at Φ = 6.07° S. The analysis shows the annual hour index for a longitudinal evaluation between two PV rows (h = 2 m, GCR = 0.3, γ = 0°, bif = 0.75) under different tilt angles ranging from 0° to 90°.

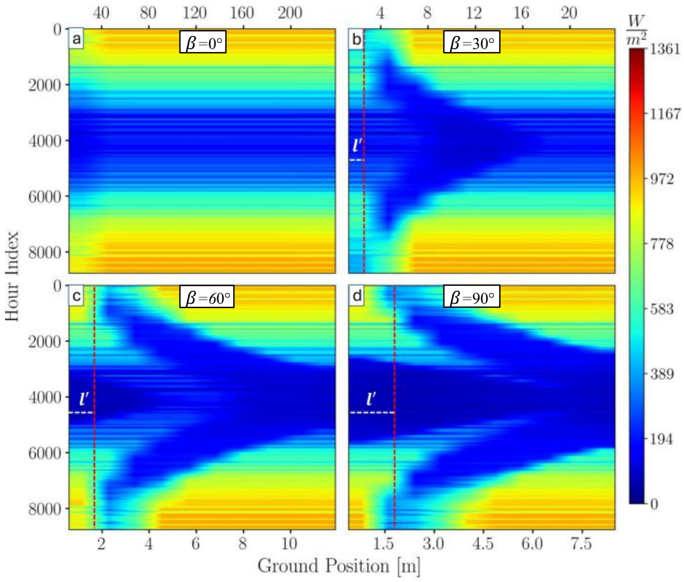

Figure 13: Simulation of irradiance on ground level for a place located at Φ = 51.78° S. The analysis shows the annual hour index for a longitudinal evaluation between two PV rows (h = 2 m, GCR = 0.2, γ = 0°, bif = 0.75) with four different tilts.

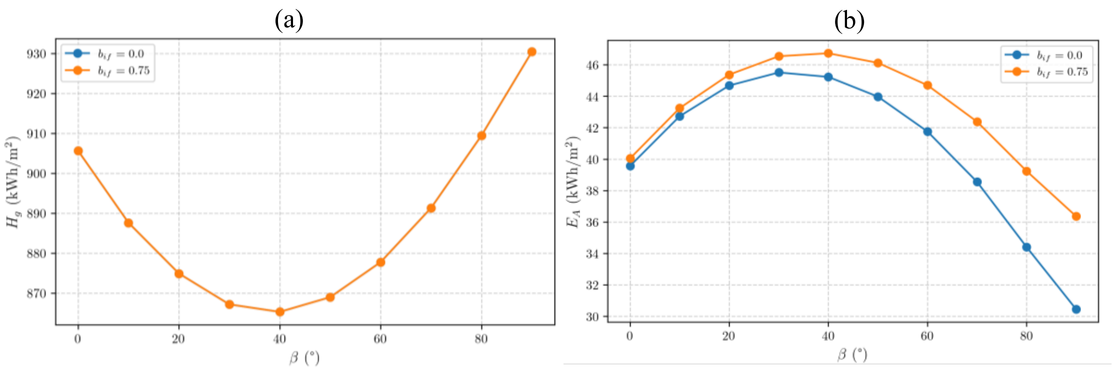

Figure 14: Plot of H_g (a) and E_A (b) vs β for two bifaciality levels, both at Φ = 51.78° S. The analysis shows the annual hour index for a longitudinal evaluation between two PV rows rows (h = 2 m, GCR = 0.2, γ = 0°, bif = 0.75) under different tilt angles ranging from 0° to 90°.

3.4 GCR

Fo this variable, the projection l' is noticeably different, since the distance d depends inversely on the GCR. For example, when GCR = 0.01, the distance d reaches values of about 200 m for a row side length l of 2.5 m (Figure 15a and 17a), this might suggest the absence of shading, but it only occurs because l' is very small compared to d. It should also be noted that H_g and E_A exhibit very sharp variations; however, this is mainly because the system area A changes, as A is inversely proportional to the GCR according to (eq. 2). Furthermore, at lower GCR values, the row spacing increases, allowing more diffuse radiation to reach the rear side of bifacial modules, which in turn enhances E.

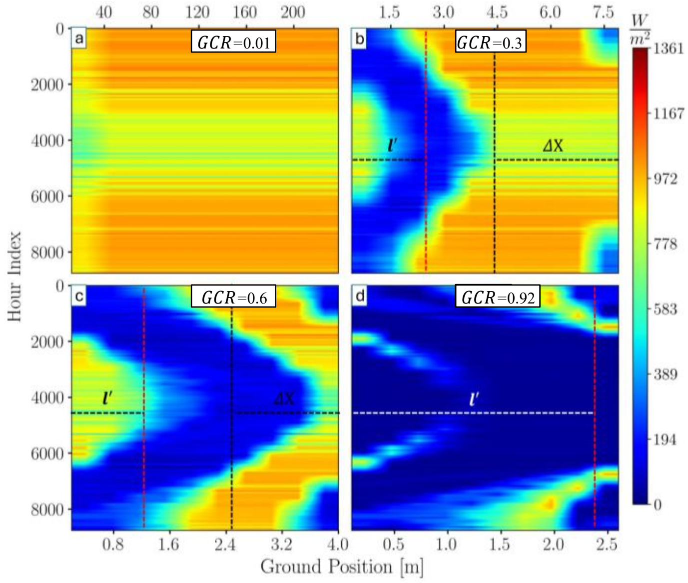

Figure 15: Simulation of irradiance on ground level for a place located at Φ = 6.07° S. The analysis presents the hour index per year for a longitudinal evaluation between two PV rows (*h*=2 m, β = 10°, γ = 0°, *bif* = 0.75) with four different GCRs.

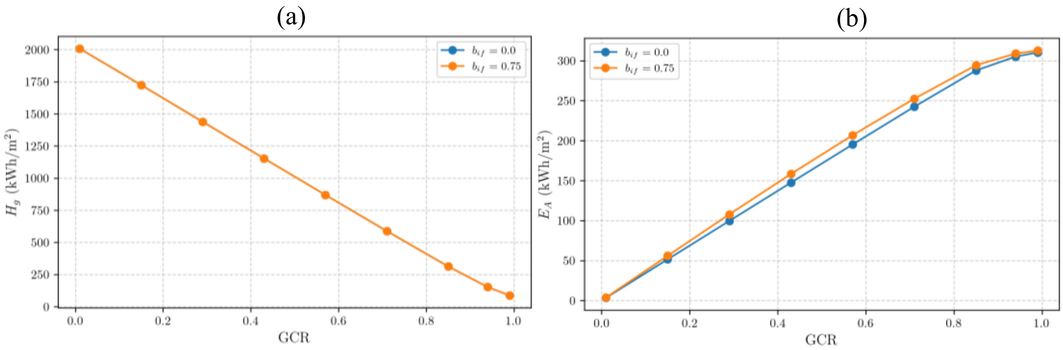

Figure 16: Plot of H_g (a) and E_A (b) vs GCR for two bifaciality levels, both at Φ = 6.07° S. The analysis shows the annual hour index for a longitudinal evaluation between two PV rows (*h*=2 m, β = 10°, γ = 0°, *bif* = 0.75) under different GCRs ranging from 0.01 to 0.99.

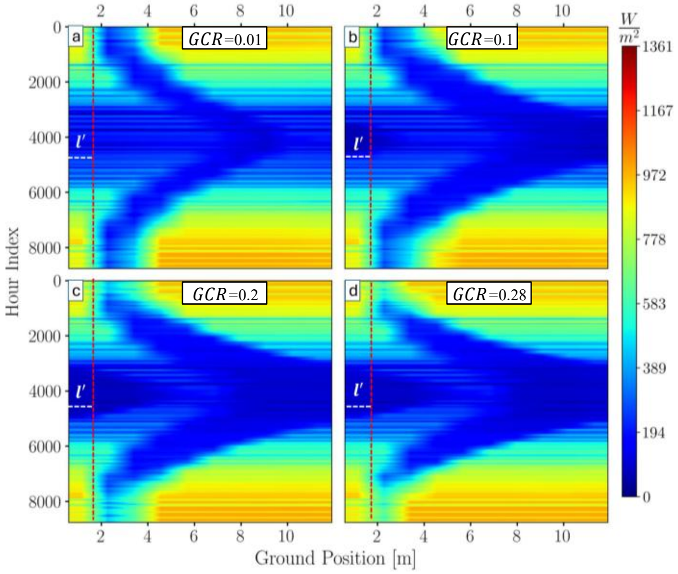

Figure 17: Simulation of irradiance on ground level for a place located at Φ = 51.78° S. The analysis presents the hour index per year for a longitudinal evaluation between two PV rows (*h*=2 m, β = 51.78°, γ = 0°, *bif* = 0.75) with four different GCRs.

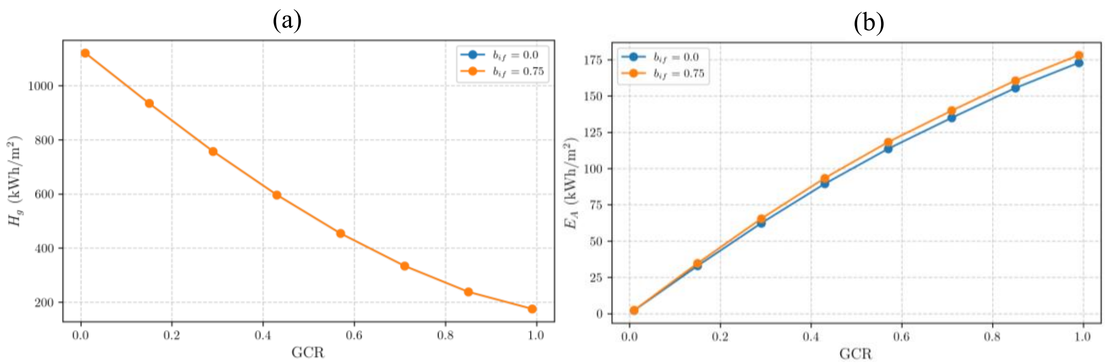

Figure 18: Plot of H_g (a) and E_A (b) for two bifaciality levels, both at *Φ* = 51.78° S. The analysis shows the annual hour index for a longitudinal evaluation between two PV rows (*h*=2 m, β = 51.78°, γ = 0°, *bif* = 0.75) under different GCRs ranging from 0.01 to 0.99.

4. Discussions

This section analyzes the results from Sections 3.1 to 3.4 for the case at latitude 6.07° S and 51.7° S. It examines how the geometric variables height (h), azimuth (γ), tilt (β), and ground coverage ratio (GCR) influence the ground irradiation H_g and annual electrical energy production E_A under monofacial and bifacial configurations.

4.1 Ground Irradiance Distribution (H_g)

Regarding h, for latitude 6.07° S, the variation $\Delta H(h)_g$ corresponds to an increase of approximately 5.3% relative to the minimum within the range from 1 m to 10 m, with the maximum occurring at h = 0 m. However, at greater heights, although the total irradiation decreases, the irradiance distribution becomes more homogeneous, as evidenced by lighter shading areas in Figure 3. Additionally, selecting h = 3 m, which is a common height used in agrivoltaic systems, results in only a 0.88% reduction in total irradiation compared to the maximum.

At latitude 51.78° S, the same parameter shows an increase of about 3.5% relative to the minimum, with the maximum at h = 1 m. Choosing h = 3 m leads to only a 0.22% reduction in total irradiation compared to the maximum, indicating a similar overall trend between both latitudes.

Regarding γ, for latitude 6.07° S, the variation $\Delta H(\gamma)_g$ corresponds to an increase of approximately 1% relative to the minimum, with maximum irradiation occurring near γ = 200°. However, at γ = 90° and 270° (Figures 7b and 7d), the irradiance distribution becomes more uniform, with a smaller total irradiation at 90°, representing only a 0.7% reduction compared to the maximum. Another notable feature is the asymmetry with respect to the south (180°) observed at 6.07° S (Figure 8a); however, at 51.78° S, the distribution becomes symmetric relative to the south (Figure 10a). The maximum irradiation occurs near γ = 180°, and the irradiance distribution also becomes more homogeneous at γ = 90° and 270° (Figures 9b and 9d), where the total irradiation at γ = 90° is about 8.8% lower than the maximum.

Regarding β, for latitude 6.07° S, the variation $\Delta H(\beta)_g$ corresponds to an increase of approximately 11.8% relative to the minimum, with maximum irradiation occurring near β= 90° he minimum at β = 0°. Thus, a higher tilt angle leads to greater H_g and a more uniform distribution of ground irradiance (Figure 12a). In contrast, for latitude 51.78° S , a (Figure 14a), the behavior is "U-shaped," with a minimum occurring at $\beta \approx 40°$, variation $\Delta H(\beta)_g$ corresponds to an increase of approximately 7.5% relative to the minimum.

Regarding GCR, for latitude 6.07°S, the variation $\Delta H(GCR)_g$ corresponds to an increase of approximately 2204.5% relative to the minimum, with maximum irradiation at GCR = 0.01 (very widely spaced). Although selecting a very small GCR would increase H_g , it would require a much larger land area for the same PV generation capacity. At latitude 51.78° S, the variation $\Delta H(GCR)_g$ shows a similar pattern, with an increase of about 539.4% relative to the minimum and maximum irradiation also occurring at GCR = 0.01.

4.2 Electrical Energy Production (E_A)

Sections 3.1, 3.2, 3.3, and 3.4 show that only three of the geometric variables considered, γ, β, and GCR, influence the annual electrical energy production when bifaciality is not considered. However, when bifaciality is included, the height h also produces a small additional increase.

Regarding h, for latitude 6.07° S, the variation $\Delta E(h)_{A,bif=0} = 0$, while for a bifaciality factor of 0.75, $\Delta E(h)_{A,bif=0.75}$ increases by 8.9% relative to the minimum, reaching its maximum at h = 4 m. The bifacial gain $\Delta_{bif} E_A(h) = E(\gamma)_{A,bif=0.75} - E(h)_{A,bif=0.75}$, varies between 1.1% and 9.8% relative to bif = 0. For latitude 51.78° S, the variation $\Delta E(h)_{A,bif=0} = 0$, while for a bifaciality factor of 0.75, $\Delta E(h)_{A,bif=0.75}$ increases by 8.9%, reaching its maximum at h = 4 m. In this case, the bifacial gain bifacial gain $\Delta_{bif} E_A(h) = E(\gamma)_{A,bif=0.75} - E(h)_{A,bif=0.75}$ varies between 4.8% and 5.3% relative to bif = 0.

Regarding γ, for latitude 6.07° S, the variation $\Delta E(\gamma)_{A,bif=0}$ represents 2.4% of its minimum value, while $\Delta E(\gamma)_{A,bif=0.75}$ represents 2.3%. The maximum occurs near γ = 25° for bif = 0 and at γ = 45° for bif = 0.75. The bifacial gain $\Delta_{bif} E_A(\gamma) = E(\gamma)_{A,bif=0.75} - E(\gamma)_{A,bif=0.75}$ varies between 1.1% and 9.8%.

It is worth noting that, for installations in the southern hemisphere, the azimuth angle is commonly set to 0°. However, the percentage difference in E_A between γ = 0° and γ = 45° is less than 0.1% for bif = 0 and about 0.44% for bif = 0.75, possibly due to local conditions such as cloudiness. Moreover, at γ = 90°, where shadows are smaller and irradiance on ground level is more uniform throughout the year, E_A is reduced by only 0.67% relative to the maximum without bifaciality, and by 0.44% considering bif = 0.75.

At latitude 51.78° S, the variation $\Delta E(\gamma)_{A,bif=0}$ represents 2.4% of its minimum value, while $\Delta E(\gamma)_{A,bif=0.75}$ represents 173.8%. The maximum occurs near γ = 0° for bif = 0 and a bif = 0.75. The bifacial gain $\Delta_{bif} E_A(\gamma) = E(\gamma)_{A,bif=0.75} - E(\gamma)_{A,bif=0.75}$ varies between 5.2% and 31.4%.

Regarding β, for latitude 6.07° S, the variation $\Delta E(\beta)_{A,bif=0}$ represents 2.4% of its minim, while $\Delta E(\beta)_{A,bif=0}$ reaches 32%, with the maximum again occurring at β = 0° up to 15°, either with bif = 0 or 0.75. The bifacial gain $\Delta_{bif} E_A(\beta) = E(\beta)_{A,bif=0.75} - E(\beta)_{A,bif=0.75}$ oscillates between 1.1% and 9.8% relative to bif = 0. At latitude 51.78° S the variation $\Delta E(\beta)_{A,bif=0}$ represents 49.5% of its minim, while $\Delta E(\beta)_{A,bif=0}$ reaches 28.5%, with the maximum occurring at β = 35° for both bif = 0 and 0.75. The bifacial gain $\Delta_{bif} E_A(\beta) = E(\beta)_{A,bif=0.75} - E(\beta)_{A,bif=0.75}$ oscillates between 1.2% and 19.4% relative to bif = 0.

For latitude 6.07° S, the variation $\Delta E(GCR)_{A,bif=0}$ represents 8923.6% of its minimum value, while $\Delta E(GCR)_{A,bif=0.75}$ represents 8286.8%. The bifacial gain $\Delta_{bif} E_A(GCR) = E(GCR)_{A,bif=0.75} - E(GCR)_{A,bif=0.75}$ oscillates between 5.9% and 8.4% relative to bif = 0. It is important to note that the system area varies inversely with the GCR (eq.2). Therefore, as GCR increases, the module rows become closer, resulting in a smaller total area. At latitude 51.78° S, the variation $\Delta E(GCR)_{A,bif=0}$ represents 7670.1% of its minimum value, while $\Delta E(GCR)_{A,bif=0.75}$ represents 7424.1%. The bifacial gain $\Delta_{bif} E_A(GCR) = E(GCR)_{A,bif=0.75} - E(GCR)_{A,bif=0.75}$ oscillates between 3.0% and 6.4 % relative to bif = 0.

5. Conclusions

The geometric parameters $h, \gamma, \beta,$ and GCR have interrelated effects on ground irradiance σ_{xt}, annual ground irradiation H_g, and annual electrical energy production E_A under monofacial and bifacial configurations.

Ground irradiance σ_{xt} and H_g are not affected by bifaciality (bif), while E_A becomes sensitive to h only when $bif \neq 0$, increasing by up to 9.8% for $bif = 0.75$ at 6.07° S compared to bif = 0, and by up to 5.3% at 51.78° S due to additional diffuse and albedo radiation.

At 51.78° S, σ_{xt} becomes more homogeneous with summer months bring longer daylight and greater diffuse reflection, while winter months show extended but smoother shading, resulting in softer annual transitions in H_g, lower contrast between shaded and lit zones, and more stable bifacial gains compared with tropical latitudes.

For γ, latitudes show similar trends, with maximum energy near $\gamma = 180°$, while $\gamma = 90°$ and 270° orientations provide uniform ground irradiance with an energy loss below 1% at 6.07° S relative to the maximum value.

The tilt angle β influences the optimal production of E_A, ranging from 0°to 10° at 6.07° S and around 35° at 51.78° S, ensuring a balance between shading, irradiance homogeneity, and annual energy yield. However, as β increases, the shadows become shorter and lighter, resulting in higher H_g, with a rising trend at 6.07° S and a U-shaped behavior at 51.78° S.

The GCR exerts the strongest influence. Lower values increase E_A and improve uniformity, but since area A varies inversely with GCR, this must be evaluated carefully. Although small GCR values enhance albedo contribution, they demand larger land areas, reducing efficiency. Therefore, the goal is to achieve greater irradiance homogeneity with minimal energy loss, maintaining sufficient height for crops and efficient land use.

To obtain better overall performance, it is recommended to adopt configurations that ensure high irradiance uniformity with minimal energy loss, maintaining adequate height for crop cultivation and efficient land use. This can be achieved with $h \approx 3$ m, $\beta = 0°–10°$, GCR close to $GCR_{max} = 0.92$, and $\gamma = 90°$ or 270° at 6.07° S, and with $h \approx 4$ m, $\beta \approx 35°$, GCR close to $GCR_{max} = 0.28$, and $\gamma = 90°$ at 51.78° S, providing bifacial gains and more homogeneous ground shading throughout the year, although higher GCR values help minimize unused space but must remain below GCR_{max} to avoid inter-row shading, since excessive density may reduce the available cultivation area.

6. References

Alegre-Bravo, A., Stedman, R.C. and Anderson, C.L. (2025) 'Rethinking the role of indicators for electricity access in Latin America: Towards energy justice', *Applied Energy*, 379. Available at: https://doi.org/10.1016/j.apenergy.2024.124877.

Asa'a, S. *et al.* (2024) 'A multidisciplinary view on agrivoltaics: Future of energy and agriculture', *Renewable and Sustainable Energy Reviews*, 200. Available at: https://doi.org/10.1016/j.rser.2024.114515.

REN21 Secretariat (2024) *RENEWABLES 2024 GLOBAL STATUS REPORT – GLOBAL OVERVIEW*. Paris. Available at: https://www.lerenovaveis.org/contents/lerpublication/2024_abr_ren21_renewables-2024--global-status-report.pdf (Accessed: 19 July 2024).

Ko, D.-Y. *et al.* (2023) 'Agrivoltaic Farming Insights: A Case Study on the Cultivation and Quality of Kimchi Cabbage and Garlic', *Agronomy*, 13(10). Available at: https://doi.org/10.3390/agronomy13102625.

Russo, C. *et al.* (2025) 'The global energy challenge: second-generation feedstocks on marginal lands for a sustainable biofuel production', *Chemical and Biological Technologies in Agriculture*, 12(1). Available at: https://doi.org/10.1186/s40538-025-00729-7.

Semeraro, T. *et al.* (2024) 'Shading effects in agrivoltaic systems can make the difference in boosting food security in climate change', *Applied Energy*, 358. Available at: https://doi.org/10.1016/j.apenergy.2023.122565.

Walston, L.J. *et al.* (2022) 'Opportunities for agrivoltaic systems to achieve synergistic food-energy-environmental needs and address sustainability goals', *Frontiers in Sustainable Food Systems*, 6. Available at: https://doi.org/10.3389/fsufs.2022.932018.

Yavari, N. *et al.* (2021) 'The effect of light quality on plant physiology, photosynthetic, and stress response in Arabidopsis thaliana leaves', *PLoS ONE*, 16(3 March). Available at: https://doi.org/10.1371/journal.pone.0247380.